DOI: 10.1002/ente.201200011

Fast Screening of the Optimal Polymer Ratio for Organic Solar Cells Using a Spray-Coating Deposition Method for the Fullerene Mixture

Jae-hyeong Lee, Takashi Sagawa,* and Susumu Yoshikawa[a]

Bulk-heterojunction organic solar cells generate electrical power from light absorption in the active layer and consist of a mixture of electron donor and acceptor materials. The donor/acceptor ratio is one of the critical parameters that determines the electrical characteristics of bulk-heterojunction solar cells. Therefore, the optimal ratio of the donor/acceptor must be determined to achieve maximum efficiency in bulk-heterojunction solar cells. In this work, modified spray- or mist-coating methods are applied to control the donor/acceptor ratio systematically and continuously. The feasibility of this processing method for polymer-ratio screening is investigated by monitoring the morphological and optical properties of polymer solar cells based on poly(3-hexylthiophene) (P3HT)/[6,6]-phenyl C61 butyric acid methyl ester (PCBM). Finally, the optimum ratio of P3HT/PCBM is obtained by increasing the ratio of P3HT/PCBM gradually. This study provides a strong and practical screening method to define the critical mixture ratio among the enormous number of polymer–fullerene combinations.

Introduction

Recent developments in organic photovoltaics (OPVs) have been achieved by the discovery of new organic donor/acceptor materials and the development of suitable coating processes. The synthesis of new polymer materials makes up much of the recent work. The most impressive high-performance polymers are those designed by Yu et al., which are composed of thieno-[3,4-b]-thiophene (TT) and benzodithiophene (BDT) alternating units.[1–3] OPVs with bulk-heterojunction (BHJ) active layers comprised of TT-BDT copolymer and [6,6]-phenyl C71 butyric acid methyl ester (PC71BM) are capable of reaching power conversion efficiencies (PCEs) of over 7%.[3] Although progress in alternative acceptors has not been as remarkable as that of donor polymers, the use of modified fullerene derivatives such as bis- and tris-PCBM has brought about a significant efficiency enhancement owing to the higher energy of the lowest unoccupied molecular orbital (LUMO) and concomitant increase in open-circuit voltage.[4,5]

However, when new donor/acceptor materials are synthesized, hundreds of experiments are required to determine an optimal ratio of the mixture for achieving the best device characteristics in a BHJ solar cell. The spin-coating method, which is the most commonly used coating technique, is not desirable for repeated screening experiments of a new material because of the relatively large amount of wasted solution and the individual manner of preparation. Other solution-based processes recently used for the fabrication of OPVs, such as screen printing,[6] doctor blading,[7,8] and spray coating,[9–16] are compatible with roll-to-roll or large-scale manufacturing[17–21] but are not suitable to screen the optimum donor/acceptor ratio. Alstrup et al. demonstrated that slot-die coating enables the optimum donor/acceptor composition to be obtained.[22] Recently, Teichler et al. reported a combinatorial screening method for polymer/fullerene blends by inkjet printing.[23] However, we still need to investigate the effect and distribution of the components by screening in case the donor/acceptor blend is insufficiently mixed.

We report a new screening tool to find the optimum donor/acceptor ratio by using the fine-channel mist-spray deposition (FCMSD) method. FCMSD is a simple coating method in which the liquid solution is ultrasonically atomized and the aerosol droplets are transferred onto the substrate using a carrier gas. This method is effectively a modification of chemical vapor deposition (CVD), which is a chemical process used to produce high-purity, high-performance thin films in the semiconductor industry.[24–27] Recently, the CVD method was also used to deposit transparent ZnO thin films.[28,30] However, in our experimental configuration, FCMSD differs from CVD as the FCMSD process operates by the deposition of the donor and/or acceptor spray coating using gas pressure without chemical reaction of the precursors.

In this report, we introduce and explain a thin-film-deposition process, FCMSD, which allows us to control the volume of donor/acceptor from each channel accurately. A mixture of poly(3-hexylthiophene) (P3HT) and [6,6]-phenyl C61 butyric acid methyl ester (PCBM) as polymer and fullerene, respectively, was selected because it is one of the most widely used and examined mixtures of OPVs. As it has been report-

---

[a] *J.-H. Lee, Prof. T. Sagawa, Prof. S. Yoshikawa*
Institute of Advanced Energy, Kyoto University
Gokasho, Uji, Kyoto 611-0011 (Japan)
E-mail: t-sagawa@iae.kyoto-u.ac.jp

ed that the P3HT/PCBM ratio producing the highest device efficiency is approximately 1:0.8, we investigated the evolution of the efficiency and polymer morphology as the PCBM/P3HT ratio was incrementally increased.[30–36] We examined the basic characteristics of FCMSD to establish reproducibility before combinatorial screening. On the basis of these results, we explain why FCMSD can be a strong and practical screening method to define the critical ratio of the mixture by one-time preparation of the solutions for a certain donor/acceptor pair to discern among the numerous polymer–fullerene combinations.

Results and Discussion

Figure 1 shows a schematic illustration of the FCMSD apparatus used in our experiment. A linear-source nozzle was designed to control a uniform flow rate of the carrier gas (N_2) on a large scale. The donor (P3HT) and acceptor (PCBM) solutions are atomized in two separate mist sources. The mists from the two sources are transferred to the nozzle using the N_2 carrier gas and combined prior to deposition onto the substrate. The substrate stage moves perpendicular to the nozzle aperture.

The device performance of the deposited films was investigated based on the common device configuration: glass–ITO (indium tin oxide)/PEDOT:PSS [Poly(3,4-ethylenedioxythiophene) poly(styrenesulfonate)]/P3HT:PCBM/LiF/Al. The film is formed by the spread of droplets and the combination of adjacent droplets. The film morphology is usually affected by the properties of the solution, such as vapor pressure, boiling point, and surface tension, as well as the flux of the droplets and ambient conditions.[9–16] However, in FCMSD, unlike spray coating, the film morphology is very sensitive to the flux of the droplets because the distance from the nozzle to the substrate is fixed at a short distance for more effective coating. Therefore, we considered the movement of droplets between the nozzle and the substrate carefully. In our system, the moving substrate was heated to 110 °C to ensure that the active layer was thoroughly dried and for reproducibility. It has previously been reported that drying at lower temperatures for a significantly longer times is more favorable for the formation of ordered crystallites in the active layer.[2,11,37,38] However, there are exceptional cases in which heating the substrate at a higher temperature leads to a highly ordered morphology.[14,39–41] At the same time, it must be considered that FCMSD, like spray coating, requires the minimization of the contact angle for highly interconnected P3HT and PCBM domains. In pretests, the performances of devices constructed by using FCMSD with a substrate heated to a high temperature were quite low ($<0.5\,\%$) as expected, even with the use of a well-mixed donor/acceptor solution. Therefore, an additional solvent annealing method was used in conjunction with heating the substrate to compensate for losses that resulted from the use of a hot substrate.[15] Solvent annealing was shown to solve the problem of the uneven and rough surface, which was attributed to fast drying.[15] With the use of solvent annealing in conjunction with FCMSD, we successfully obtained a regular, pinhole-free morphology. Figure 2 shows optical images before and after additional solvent coating with *o*-dichlorobenzene (DCB). To study the morphology of the surface clearly, we investigated the surface of an Al electrode coated with approximately 30 nm of the material. The white areas and lines in Figure 2 a show a sparse distribution of P3HT:PCBM droplets. After additional solvent coating, the characteristic peaks of the surface profile (green line) in Figure 2 a disappeared. This means that the uneven surface becomes smooth (Figure 2 b).

We investigated the optimal thickness for an organic solar cell. This was determined by considering the performance of OPVs, and reproducibility was one of the most important factors considered. For fast screening of an optimal ratio of polymer/fullerene mixture for BHJ organic thin-film solar cells, it was important to obtain consistent results, even at the expense of a somewhat lower efficiency. The optimal thickness of the active layer can be varied by changing the coating process.[15,22,42] In particular, this method, in which the active layer is formed by the accumulation of dried droplets, gives rise to a thicker optimal active layer because a thicker droplet stacking serves to limit pinholes and cracks.[22,42] Figure 3 shows the surface morphologies of active layers with different thicknesses. As the coating process was repeated for a given substrate area, the thickness of the active layer gradually increased by approximately 30 nm due to exposure to dryness. The droplets were deposited sequentially in that the droplets from the latest coating exposure covered the previous layers as shown in Figure 3 a, c, and e. Here, the blue area, namely, the PEDOT:PSS layer, was gradually covered with P3HT:PCBM droplets as the coating exposure increased. The surface profiler images after the

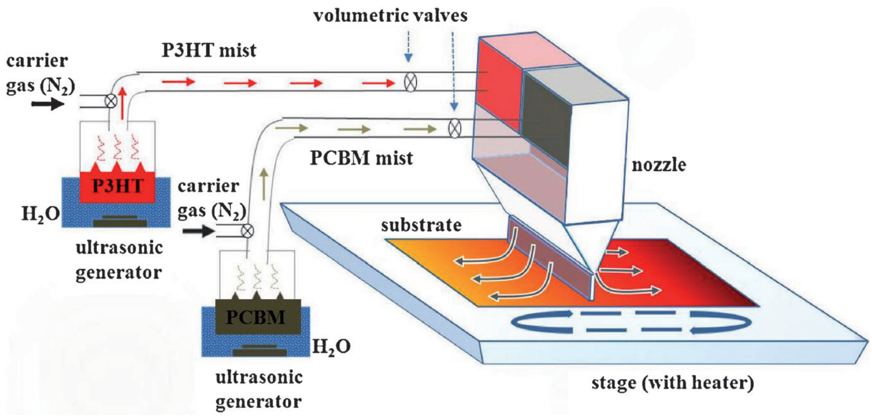

Figure 1. Schematic illustration of FCMSD apparatus.

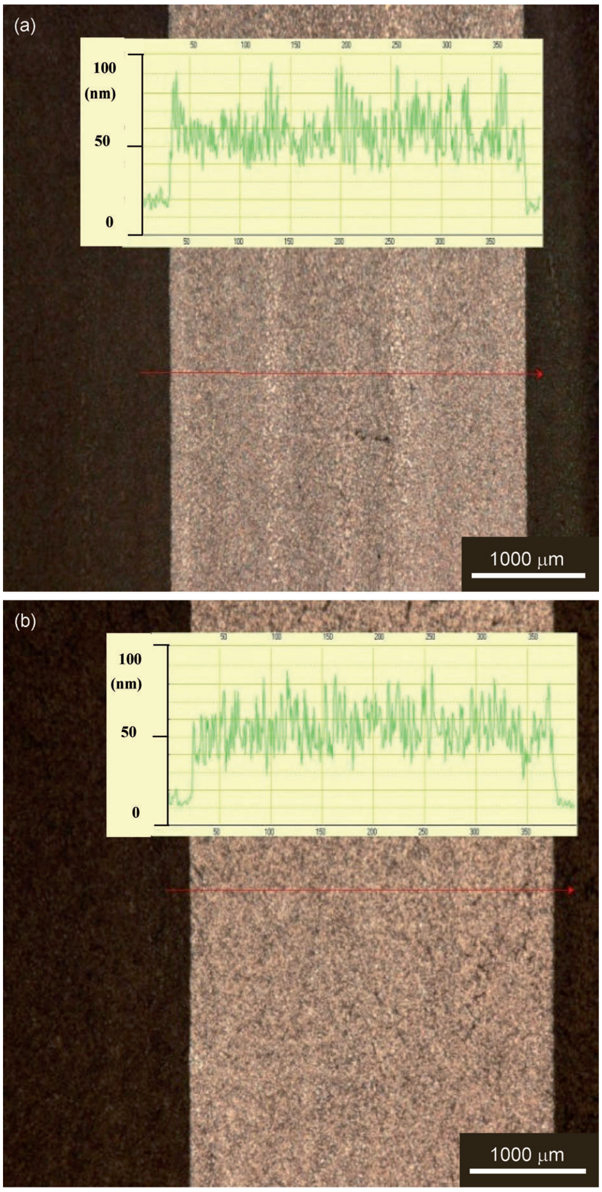

Figure 2. Optical images of the glass-ITO/PEDOT:PSS (spin coating)/P3HT-PCBM (FCMSD)/LiF/Al device (a) before and (b) after additional solvent coating with DCB.

additional coating with DCB are presented in Figure 3b, d, and f. Owing to the reduction of residues and pinholes, the scale of Figure 3b, d, and f is smaller than that of Figure 3a, c, and e. The minimum thickness of the active layer for stable and reproducible performance was determined to be around 310 nm with a root mean square (rms) roughness of 45 nm for the FMSCD method with additional DCB solvent coating. More coating by using FCMSD does not correlate to a better peak-to-valley value. Instead, the thicker active layer does not dissolve and residues remain. Moreover, the absorption is also affected by a thicker layer. Therefore, we sought to achieve a more appropriate thickness to cover the pinholes and block the shunts.

The peak-to-valley value of 300 nm is higher than that of the spin-coated material. However, in the case of FCMSD, it is important to connect the isolated droplets to each other and fill the pinholes, even though the thicker active layer of over 100 nm generally seems to be unfavorable for forming a favorable carrier path. Therefore, other groups who have been researching spray coating obtained high performances with active layers of 150–300 nm thickness.[22,23]

The performances of devices with active layers approximately 300 nm thick before and after additional DCB coating is shown in Figure 4 . In devices with DCB treatment, the variation of the efficiency of the devices decreased, and the short-circuit current density (J_{sc}) was remarkably stabilized. However, devices without DCB solvent coating showed a high deviation of J_{sc}, even though the efficiency often reached above 1%, which is the average for devices with DCB coating. The additional solvent coating prevents current loss through pinholes, which can be formed in mist coating.[15,22,42]

The distribution of sulfur (S) and carbon (C) in the P3HT:PCBM active layer (400×400 μm) is shown in Figure 5, as measured by energy dispersive spectroscopy (EDS) by using SEM. For screening, proof is required that the p/n content in the active layer coated by using FCMSD is exactly consistent with the target composition. In the P3HT:PCBM active layer, S originates from P3HT, which means that we can estimate the distribution of P3HT from the distribution of S. It is hard to distinguish which areas represent P3HT and PCBM by searching for dots of C because both P3HT and PCBM are mainly composed of C. Therefore, we compared the relative proportion of S and C in the devices, which were fabricated by using FCMSD (fab.) and theoretically calculated (cal.) as the PCBM/P3HT ratio was increased from 0.33 to 1.00 with in steps of 0.11. By comparison of the results, we confirmed that the proportion of S and C sprayed by the computer-controlled nozzle ($S_{cal.}$, $C_{cal.}$) did not deviate significantly from the proportion of S and C deposited on the substrate ($S_{fab.}$, $C_{fab.}$) until the PCBM/P3HT ratio reached 0.55. When the PCBM/P3HT ratio was greater than 0.55, $C_{fab.}$ was generally underestimated and $S_{fab.}$ overestimated compared to $S_{cal.}$ and $C_{cal.}$. The deviation between the calculated and experimental values indicates that the deposited amount of PCBM was slightly lower than the amount of sprayed PCBM. This phenomenon is attributed to the difference between the sprayed quantities and the quantities that are coated onto the substrate. As the PCBM/P3HT ratio is controlled by the amount of PCBM injected into the constant P3HT volume, the increased PCBM/P3HT ratio means that the total flow rate is increased. When the flow rate increases with the increased PCBM/P3HT ratio, the amount of uncoated PCBM also increases simultaneously. However, the overall trend did not change remarkably although the PCBM/P3HT ratio increased gradually.

The spatial distribution of S and C in the P3HT:PCBM active layer was further analyzed by observing cross-sectional views by using EDS. For clarity, the active layer was coated repeatedly until its thickness reached 3 μm. We found that

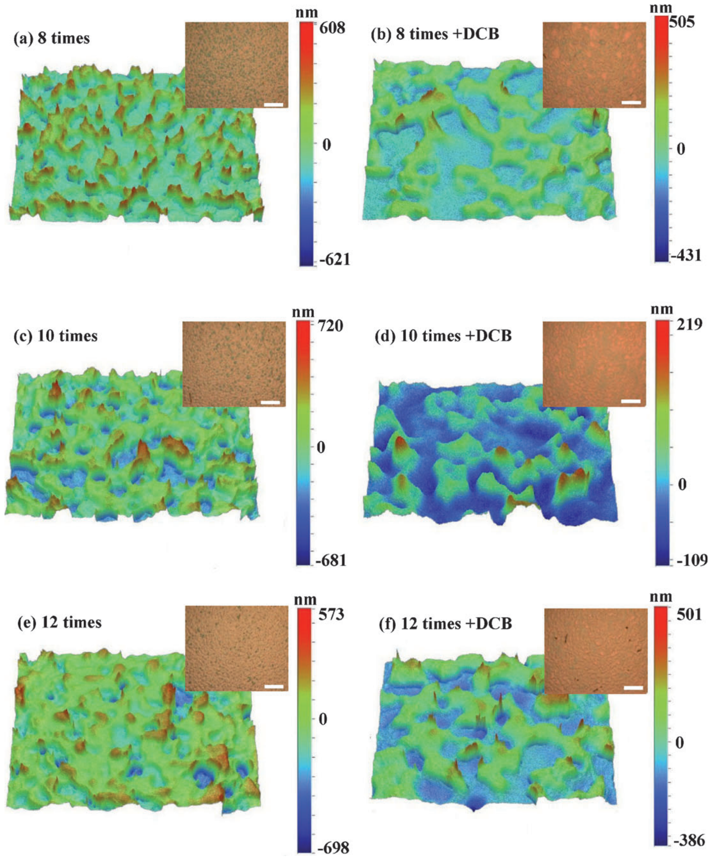

Figure 3. Surface topographies of glass-ITO/PEDOT:PSS (spin coating)/P3HT-PCBM (FCMSD) with (a, c, e) and without (b, d, f) additional solvent coating. Devices b, d, and f were coated with DCB. The scale bar is 100 μm and the color scan areas are 93.8×125.1 μm^2.

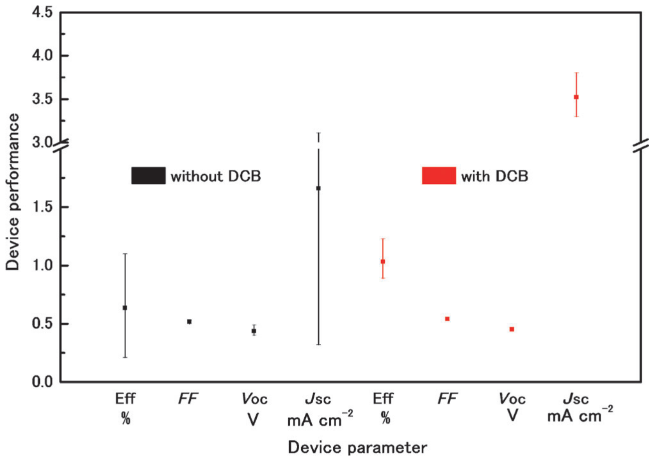

Figure 4. Comparison of performance of devices with and without additional DCB coating.

the distribution of S is unbalanced and abundant near the bottom of the layer as shown in Figure 6. This observation is supported by the optical image shown in Figure 7 a, which shows large PCBM clusters on the surface of the active layer.

Large densities and sizes of crystal grains were found when the P3HT:PCBM mixture contained excess PCBM.[36] This phenomenon can be explained as follows: after the P3HT:PCBM aerosol scatters from the nozzle, the PCBM component, which has a high solubility in chlorobenzene (CB), dries faster on the hot substrate. Subsequently, the dried PCBM droplets are lifted by the ascending air current, which originates from the hot substrate, and this leads to the vertical separation of P3HT and PCBM. This phenomenon is the opposite of the case for spin coating, in which the PCBM component segregates toward the solvent-rich side of the BHJ film.[43] In FCMSD, the donor and acceptor are divided into two phases horizontally and the structure of the active layer is far from the ideal BHJ nanostructure. Consequently, without the formation of a proper BHJ nanostructure, the advantages of BHJ nanostructures such as shorter exciton diffusion ranges and the maximization of enhanced pathways for both charge carriers to the relevant electrodes are not realized. Interestingly, the large crystal grains disappeared after additional DCB solvent coating (Figure 7) as it allowed the active layer matrix to redissolve such that isolated active layer droplets could become interconnected in the presence of the DCB droplets.[13,15] It could be expected that the additional solvent coating helps to shift

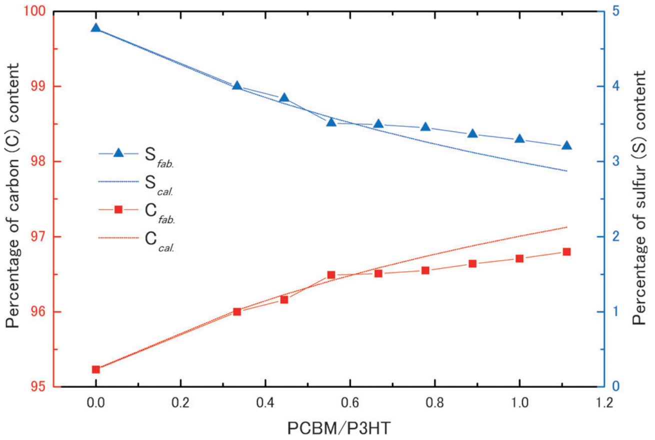

Figure 5. Comparison of C and S content in the active layer of the fabricated ($S_{fab.}$, $C_{fab.}$) and calculated devices ($S_{cal.}$, $C_{cal.}$).

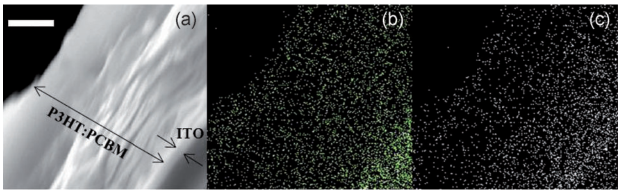

Figure 6. EDS analysis of C and S in a thick active layer. A SEM image is shown in (a), and the C and S content are shown in (b) and (c) respectively. The scale bar is 1 μm.

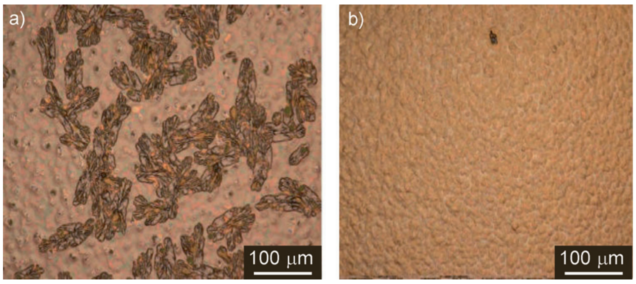

Figure 7. Optical images of the surface of the active layer (a) before and (b) after additional solvent coating.

and rearrange the bulk as well as the surface of the active layer.

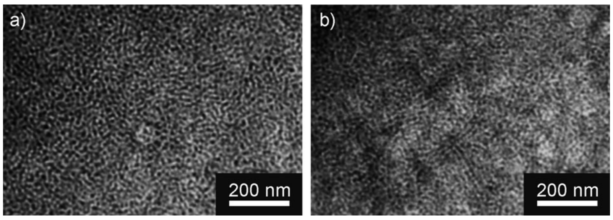

Figure 8. TEM images of P3HT-PCBM(FCMSC)/additional solvent coating with different P3HT/PCBM ratios: (a) 1:0.33 and (b) 1:1.

To investigate the variation of the bulk nanoscale morphology in the active layers formed from various ratios of PCBM/P3HT in the range of 0.33–1.00, TEM images of the BHJs were observed (Figure 8). It has been reported that the brightness contrast of P3HT crystals observed in TEM is caused by the lower density of P3HT ($1.10\,\mathrm{g\,cm^{-3}}$) than that of PCBM ($1.50\,\mathrm{g\,cm^{-3}}$).[44,45] It is known that the most pronounced change in the TEM image of the thermal- or solvent-annealed device is the increased contrast between dark and bright areas and the appearance of bright fibrillar P3HT crystals over the entire film.[46] In the image shown in Figure 8a, elongated fibrillar P3HT crystals are not as clear as those in Figure 8b, even after thermal and solvent annealing. We presume that the growth of P3HT is restricted when the amount of PCBM in the P3HT:PCBM matrix is quite low. In addition, PCBM nanocrystals cannot aggregate into PCBM-rich domains. This allows us to determine the origin of the changes in morphology during the annealing process and to understand which component moves first. Two theories have been proposed to explain this change in morphology. The first theory is that shorter fibrillar-like P3HT crystals already exist in the pristine film and the annealing process supports their combination to grow into longer fibrils, which build barriers that hamper the extensive diffusion of PCBM molecules into the P3HT network.[46] The second theory is that during annealing, isolated molecules of PCBM begin to diffuse into larger aggregates and P3HT aggregates can be converted into P3HT crystallites in PCBM-free regions.[47] Considering the TEM image and the XRD patterns (Figure 12), the P3HT crystallites are enhanced even in films with smaller amounts of PCBM. Therefore, we believe that short P3HT crystals could be elongated readily by thermal annealing, even before PCBM-free regions are formed. However, it is expected that PCBM aggregation, which supports electron transport, is established more clearly when enough PCBM is present (following the results in Figure 8b).

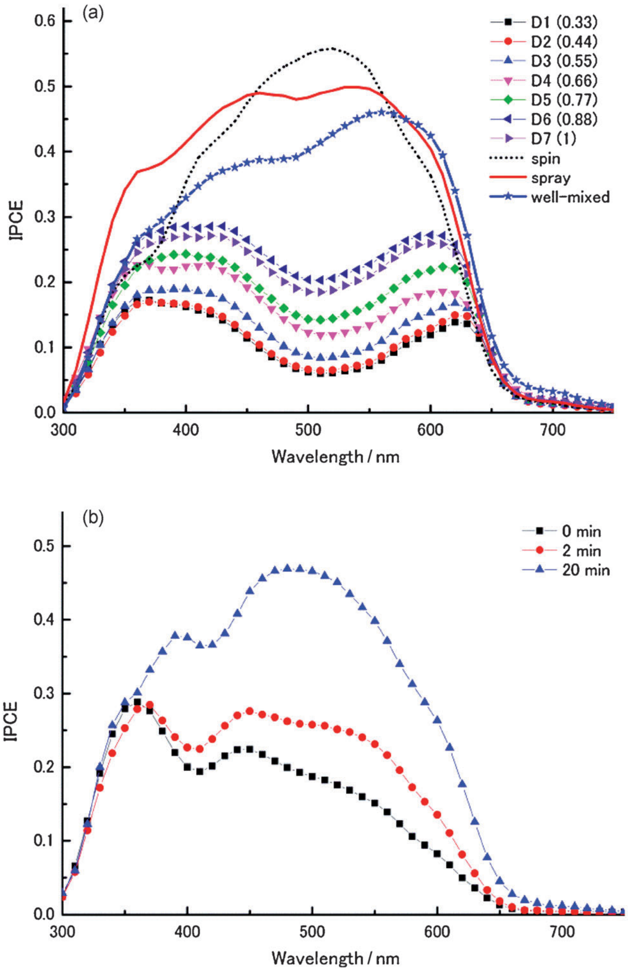

Figure 9. (a) IPCE comparison of glass-ITO/PEDOT:PSS/P3HT-PCBM/additional solvent coating/LiF/Al devices ($100\,\mathrm{mW\,cm^{-2}}$). (b) IPCE comparison of three spin-coated devices with different mixing times.

The incident photon-to-current efficiency (IPCE) curves of the devices are shown in Figure 9a for PCBM/P3HT ratios over the range of 0.33–1.00 in increments of 0.11 (designated as D1–D7). The combinatorial devices fabricated by using FCMSD were compared to the devices fabricated by using spin and spray coating.[15] The devices fabricated by using mist coating have lower efficiencies in the range of 450–550 nm, and the photons absorbed at these wavelengths make substantial contributions to the overall efficiency in devices fabricated by using spin and spray coating. The IPCE curves of the mist-coated devices show an M-shaped curve for which the lowest point is at 520 nm in all devices. We consider that this phenomenon is a result of three aspects:

the thickness of the active layer, the temperature of the substrate, and the poor blending of the donor and acceptor components. First, the thickness of the active layer was ruled out because an M-shaped curve was not obtained for a spray-coated device with an active layer thickness of approximately 700 nm.[42] The high temperature (110 °C) of the substrate may also cause the M-shaped curve by leading to the formation of smaller P3HT crystallites. However, devices fabricated by using FCMSD, with well-mixed P3HT:PCBM solutions, even if the device is heated to 110 °C, do not show this M-shaped curve (Figure 9 a). To investigate the effect of poorly mixed P3HT:PCBM solutions, we prepared three spin-coated devices with different mixing times (0, 2, and 20 min), in which a longer mixing time connotes a better blend of the P3HT and PCBM components. Figure 9 b shows the IPCE characterization of the prepared devices. A similar trend was found in the IPCE shape for all three devices even though the M-shaped curves are not well matched. This means that poorly blended P3HT:PCBM mixtures affect the IPCE negatively. This hypothesis is supported by the results of EDS and the optical images in Figures 6 and 7, respectively.

Images of the laser-beam-induced current (LBIC) are shown in Figure 10, to visualize any spatial non-uniformities in thin film solar cells. The width of the device was 1.5 mm, which is smaller than our conventional devices to account for the resolution of our equipment and deterioration during measurements. The darker areas between the devices show the boundaries between each of the seven devices formed with different ratios of the mixtures in the active layer. However, the boundary between D1 and D3 is ambiguous. This is attributed to residues from the nozzle that were scattered between D1 and D3 when the nozzle returned to its original position. This extra coating could affect the thickness of the active layer of the device and cause a change in the ratio of the mixture in the active layer for repeated cycles. However, the error was negligible below ten repeated cycles, and it could be avoided by creating a marginal space in the front. In D6, a white area occupies a large area, which indicates a high current density generated with light exposure. The distribution of white in D5, D6, and D7 is related to good device performance, which is also shown in Figure 13 and discussed later.

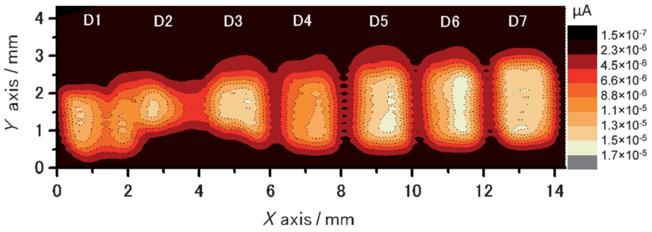

Figure 10. LBIC images of a fast-screen-coated device.

The photoluminescence (PL) intensity according to the PCBM fraction is shown in Figure 11. The quenching of fluorescence of the donor/acceptor composition is an important factor to find an efficient donor/acceptor combination. However, it does not necessarily mean that stronger PL quenching leads to more efficient solar cells. The degree of charge generation and exciton dissociation, which is related to the interfacial area of blends, can be inferred from the degree of PL quenching.[38,48] The PL intensity decreases gradually upon the addition of PCBM, and the highest peak shows a minimum for D5 and D6 for which the PL intensity is half of the maximum value of D1 (Figure 11, inset). This trend of the reduction in the PL intensity is consistent with the trend seen for spin-coated devices.[31] The shape of the PL spectrum does not change, but the intensity decreases with the increase of the amount of PCBM, with the exception of a small redshift observed for D1 and D4. This indicates that the PL is affected by residual excitons related to P3HT in the spectral region over the range of 550–850 nm. This reduction also demonstrates the efficiency of the photoinduced charge separation between the donor (P3HT) and acceptor (PCBM).[49,50]

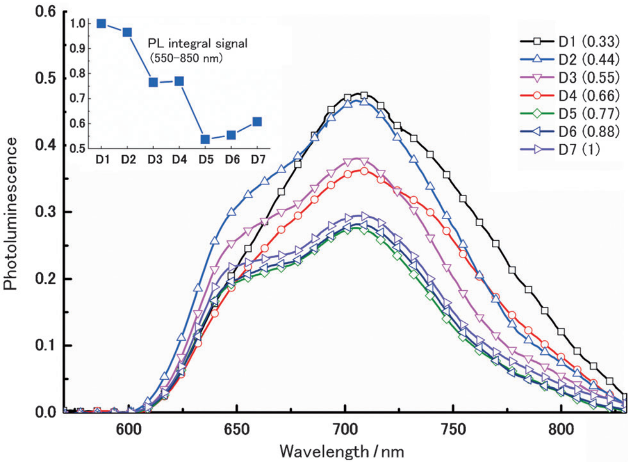

Figure 11. PL intensity according to the amount of PCBM. PL integral signal of each device is shown inset.

To investigate which PCBM/P3HT ratio is effective for enhancing the crystallization of P3HT, we measured the XRD pattern of each device (Figure 12). The height of the peak at $2\theta = 5.4°$, which represents the crystallinity of the polymer, did not change appreciably with the changes in the blend ratios. The diffractograms of D1 and D2 show well-distinguished shapes: a low, blunt peak at $2\theta = 5.4°$ and distinct peaks at around $2\theta = 16°$. Among them, the peak at $2\theta = 16°$ indicates that the P3HT molecules remain in the amorphous P3HT:PCBM matrix.[47,51–53] The reason for these phenomena is that the aggregation of PCBM is not enough for the P3HT to crystallize when the amount of PCBM is low. The low PCBM concentration makes it more difficult for the molecules to aggregate, and sparse PCBM aggregation cannot support the formation of P3HT crystallites throughout the annealing process. This is supported by the fact that more substantial crystallite formation and more aggregated PCBM clusters were found in D7 (Figure 8).

The notable result of screening the devices formed by using FCMSD is revealed in the characteristic *J*–*V* curves

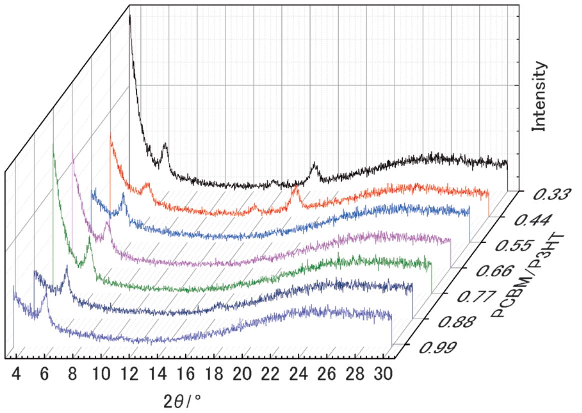

Figure 12. XRD patterns of fast-screen-coated devices fabricated by using FCMSD. The PCBM/P3HT ratios of 0.33–0.99 correspond to device numbers D1–D7 as described in the text.

(Figure 13). The resulting combinatorial device for screening fabricated by using FCMSD is shown in the inset of Figure 13. The coated area was changed slightly to match the mask available for electrode deposition. The maximum J_{sc} value is 4.75 mA cm^{-2} in D6, which shows the highest PCE. The incremental increase of PCBM component in the device series up to D6 led to increased J_{sc} values [1.59 mA cm^{-2} for D3 (1:0.55) and 4.75 mA cm^{-2} for D6 (1:0.88)]. J_{sc} is then reduced when the PCBM/P3HT ratio exceeds 1:1. This shows that high photocurrent results from the device regions composed of the P3HT:PCBM matrix with the optimum ratio.[47] This trend is consistent with the PL results shown in Figure 10. The fill factor (*FF*) also dramatically increases to 0.56 for D6, which has a PCBM/P3HT ratio of 1:0.88, compared to approximately 0.43 for D1–D3.

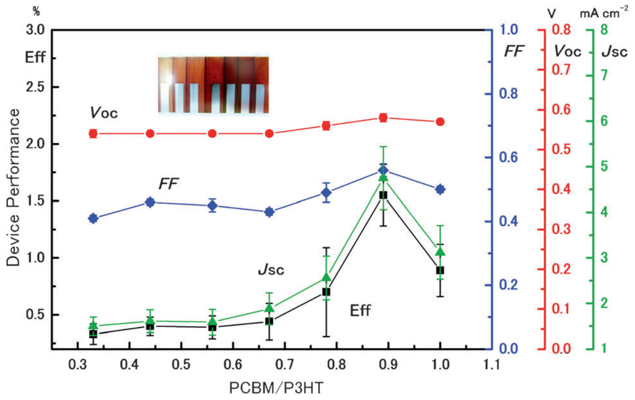

Figure 13. Device performance and characteristics of fast-screen-coated devices fabricated by using FCMSD.

Considering the complexity of making combinatorial devices on one substrate, the obtained power efficiency is relatively high. The characteristic trends of the devices also show reproducibility, even if the concentration of P3HT:PCBM solution is changed.

Conclusions

We have studied the feasibility of FCMSD as an alternative screening tool to obtain the optimum ratio of P3HT:PCBM thin-film solar cells. The desired ratio of donor/acceptor was reproducibly and accurately deposited on the substrate. However, by using just FCMSD the active layer components were poorly blended. We solved the problem by using additional solvent coating to enhance the rearrangement of the P3HT and PCBM components in the active layer. When the amount of PCBM is low, the elongation of the P3HT crystals is limited upon thermal annealing as shown in the results of XRD and TEM. Unfortunately, a poorly mixed active layer still exists after additional solvent coating, which results in M-shaped IPCE curves. Finally, the highest PCE of 1.5 % was obtained for the device with a P3HT/PCBM ratio of 1:0.88. We think that FCMSD provides the capability to screen optimum device structures, comparing favorably to other methods such as roll-to-roll processing. Furthermore, we expect that FCMSD can encourage the development of new donor and acceptor molecules for use in OPVs.

Experimental Section

For performance tests, we prepared thin films and solar-cell active layers based on a 1:0.8 mixture of P3HT (Rieke Metal) and PCBM (Nano C) dissolved in CB by using FCMSD. In the preparation of solar-cell devices, ITO-coated glass substrates (Geomatec, 5 Ω cm^{-2}) were first patterned by etching and then cleaned thoroughly with a sequence of solvents: detergent, deionized water, acetone, and isopropanol, for 10 min each in an ultrasonic bath. The cleaned substrates were purified further by oxygen plasma treatment for 10 min. The substrates were then spin coated with a filtered PEDOT:PSS solution (0.45 μm, Clevios P, HC Starck) at 4000 rpm for 60 s to produce a 40-nm-thick layer. The substrates were subsequently heated with a hotplate in air at 200 °C for 10 min to remove excess water. Solutions of the active-layer components, P3HT and PCBM, were prepared separately with concentrations of 8 mg mL^{-1} in CB and stirred in an ultrasonic bath at 50 °C for 2 h. These solutions of the active-layer components were each loaded into respective ultrasonic bottles for mist generation. The ultrasonic transducer produces a vibration with six oscillators in the water. The solution was atomized by the ultrasonic transducer (2.9 MHz), and the aerosols formed were transferred by N_2 carrier gas at a flow rate of 4 L min^{-1}. The mixed aerosols in the nozzle were supplied through the linear-source nozzle onto the heated substrate at a rate of 1.2 mL min^{-1}. The substrate temperature was fixed at 110 °C, and the number of coating exposures was set to 10. The stage was moved at a constant rate of 1 mm s^{-1}. The distance of the nozzle from the substrate was 1 mm.

In the screening experiment, the volumetric flow rate of the P3HT solution was fixed at 1.2 mL min^{-1} and the flow rate of the PCBM solution was varied to form D1–D7 at 0.11 mL min^{-1} increments, starting with 0.4 mL min^{-1} (D1) and ending with 1.2 mL min^{-1} (D7). Additional solvent-mist spray-coating was performed by spraying DCB onto the active layers at a rate of 100 μL min^{-1} at ambient temperature. The active layer was allowed to dry for approximately 10 s. Thermal annealing was performed at 150 °C for 10 min in a glove box. Lithium fluoride (10 Å) and aluminum (100 nm) were deposited by thermal evaporation under a high vacuum at 5×10^{-3} Pa. The photovoltaic characteristics were measured under a N_2 atmosphere by using an Agilent 4156C parameter analyzer under AM 1.5 G (100 mW cm^{-2}) simulated illumination by using a solar simulator with a 1000 W Xe arc lamp.

For device characterization, the thickness was measured by using an Alpha-Step IQ surface profiler (KLA-Tencor Co.), which has a precision of ±10 nm. The surface image was measured by using a Wyko NT9100 optical profiler.

UV/Vis absorption spectra were obtained by using a Shimadzu UV-1601PC UV/Vis spectrophotometer. Thin polymer films were deposited onto previously cleaned quartz slides under the same conditions used for the production of solar cells.

The 2D local characteristics of the OPVs were obtained by LBIC, which was uniquely equipped to produce quantitative maps of local quantum efficiency with relative ease. To investigate the effect of the additional solvent on the morphology of the active layer, XRD and surface profiling were used. The morphology of the active layer was observed by using TEM (JEM2100).

PL studies were carried out by using a He–Cd laser operating at 325 nm. Field-emission scanning electron microscopy (FE-SEM, JSM-6500F) and EDS (EX-23000BU) were used to investigate the distribution of the components.

Acknowledgements

The authors are indebted to Prof. Yoshinobu Tsujii of the Institute for Chemical Research, Kyoto University, for the use of the surface profiler and TEM. We thank Prof. Hideaki Ohgaki of the Institute of Advanced Energy, Kyoto University, for the use of the He–Cd laser. We are also grateful to Yoshio Masuda (TOUKI Co. Ltd.) for his advice on the design and manufacture of the FCMSD apparatus. This work was partially supported by the New Energy and Industrial Technology Development Organization (NEDO) of the Ministry of Economy, Trade, and Industry (METI), the Core Research of Evolutional Science & Technology Agency (CREST) of the Japan Science Technology Agency (JST), and the Global Center of Excellence (GCOE) Program of Kyoto University from the Ministry of Education, Culture, Sports, Science and Technology (MEXT) in Japan.

Keywords: fullerenes · optimization · polythiophenes · solar cells · spray coating

[1] Y. Liang, Y. Wu, D. Feng, S.-T. Tsai, H.-J. Son, G. Li, L. Yu, *J. Am. Chem. Soc.* **2009**, *131*, 56.
[2] Y. Liang, D. Feng, Y. Wu, S.-T. Tsai, G. Li, C. Ray, L. Yu, *J. Am. Chem. Soc.* **2009**, *131*, 7792.
[3] H.-Y. Chen, J. Hou, S. Zhang, Y. Liang, G. Yang, Y. Yang, L. Yu, Y. Wu, G. Li, *Nat. Photonics* **2009**, *3*, 649.
[4] M. Lenes, S. W. Shelton, A. B. Sieval, D. F. Kronholm, J.C. Hummelen, P. W. M. Blom, *Adv. Funct. Mater.* **2009**, *19*, 3002.
[5] M. A. Faist, P. E. Keivanidis, S. Foster, P. H. Wöbkenberg, T. D. Anthopoulos, D. D. C. Bradley, J. R. Durrant, J. Nelson, *J. Polym. Sci. Part B* **2011**, *49*, 45.
[6] S. E. Shaheen, R. Radspinner, N. Peyghambarian, G. E. Jabbour, *Appl. Phys. Lett.* **2001**, *79*, 2996.
[7] P. Schilinsky, C. Waldauf, C. J. Brabec, *Adv. Funct. Mater.* **2006**, *16*, 1669.
[8] F. Nickel, C. Sprau, M. F. G. Klein, P. Kapetana, N. Christ, X. Liu, S. Klinkhammer, U. Lemmer, A. Colsmann, *Sol. Energy Mater. Sol. Cells* **2012**, *104*, 18.
[9] B.-K. Yu, D. Vak, J. Jo, S.-I. Na, S.-S. Kim, M.-K. Kim, D.-Y. Kim, *IEEE J. Sel. Top. Quant. Electron.* **2010**, *16*, 1838.
[10] D. Vak, S.-S. Kim, J. Jo, S.-H. Oh, S.-I. Na, J. Kim, D.-Y. Kim, *Appl. Phys. Lett.* **2007**, *91*, 081102.
[11] T. Matsutani, K. Yamamoto, *J. Phys. Conf. Ser.* **2011**, *272*, 012015.
[12] R. Green, A. Morfa, A. J. Ferguson, N. Kopidakis, G. Rumbles, S. E. Shaheen, *Appl. Phys. Lett.* **2008**, *92*, 033301.
[13] H.-Y. Park, K. Kim, D. Y. Kim, S.-K. Choi, S. M. Jo, S.-Y. Jang, *J. Mater. Chem.* **2011**, *21*, 4457.
[14] G. Susanna, L. Salamandra, T. M. Brown, A. Di Carlo, F. Brunetti, A. Reale, *Sol. Energy Mater. Sol. Cells* **2011**, *95*, 1775.
[15] J. Lee, T. Sagawa, S. Yoshikawa, *Org. Electron.* **2011**, *12*, 2165.
[16] K. X. Steirer, M. O. Reese, B. L. Rupert, N. Kopidakis, D. C. Olson, R. T. Collins, D. S. Ginley, *Sol. Energy Mater. Sol. Cells* **2009**, *93*, 447.
[17] R. Søndergaard, M. Hösel, D. Angmo, T. T. Larsen-Olsen, F. C. Krebs, *Mater. Today* **2012**, *15*, 36.
[18] F. C. Krebs, *Sol. Energy Mater. Sol. Cells* **2009**, *93*, 394.
[19] F. C. Krebs, T. D. Nielsen, J. Fyenbo, M. Wadstrøm, M. S. Pedersen, *Energy Environ. Sci.* **2010**, *3*, 512.
[20] A. J. Medford, M. R. Lilliedal, M. Jørgensen, D. Aarø, H. Pakalski, J. Fyenbo, F. C. Krebs, *Opt. Express* **2010**, *18*, A272.
[21] F. C. Krebs, J. Fyenbo, D. M. Tanenbaum, S. A. Gevorgyan, R. Andriessen, B. van Remoortere, Y. Galagan, M. Jørgensen, *Energy Environ. Sci.* **2011**, *4*, 4116.
[22] J. Alstrup, M. Jørgensen, A. J. Medford, F. C. Krebs, *ACS Appl. Mater. Interfaces* **2010**, *2*, 2819.
[23] A. Teichler, R. Eckardt, S. Hoeppener, C. Friebe, J. Perelaer, A. Senes, M. Morana, C. J. Brabec, U. S. Schubert, *Adv. Energy Mater.* **2011**, *1*, 105.
[24] Y. Kamada, T. Kawaharamura, H. Nishinaka, S. Fujita, *Jpn. J. Appl. Phys.* **2006**, *45*, L857.
[25] J. G. Lu, T. Kawaharamura, H. Nishinaka, Y. Kamada, T. Ohshima, S. Fujita, *J. Cryst. Growth* **2007**, *299*, 1.
[26] A. Smith, *Thin Solid Films* **2000**, *376*, 47.
[27] J. M. Bian, X. M. Li, C. Y. Zhang, W. D. Yu, X. D. Gao, *Appl. Phys. Lett.* **2004**, *85*, 4070.
[28] H. Nishinaka, T. Kawaharamura, S. Fujita, *Jpn. J. Appl. Phys.* **2007**, *46*, 6811.
[29] T. Ikenoue, N. Kameyama, S. Fujita, *Phys. Status Solidi C* **2011**, *8*, 613.
[30] Y. Kim, S. Cook, S. M. Tuladhar, S. A. Choulis, J. Nelson, J. R. Durrant, D. D. C. Bradley, M. Giles, I. McCulloch, C.-S. Ha, M. Ree, *Nat. Mater.* **2006**, *5*, 197.
[31] Y. Kim, S. A. Choulis, J. Nelson, D. D. C. Bradley, S. Cook, J. R. Durrant, *J. Mater. Sci.* **2005**, *40*, 1371.
[32] M. T. Dang, L. Hirsch, G. Wantz, *Adv. Mater.* **2011**, *23*, 3597.
[33] H. Hoppe, N. S. Sariciftci, *J. Mater. Chem.* **2006**, *16*, 45.
[34] T. Yamanari, T. Taima, K. Hara, K. Saito, *J. Photochem. Photobiol. A* **2006**, *182*, 269.
[35] C.-K. Lee, C.-W. Pao, C.-W. Chu, *Energy Environ. Sci.* **2011**, *4*, 4124.
[36] D. Chirvase, J. Parisi, J. C. Hummelen, V. Dyakonov, *Nanotechnology* **2004**, *15*, 1317.
[37] L. Chang, H. W. A. Lademann, J.-B. Bonekamp, K. Meerholz, A. J. Moulé, *Adv. Funct. Mater.* **2011**, *21*, 1779.
[38] G. Li, Y. Yao, H. Yang, V. Shrotriya, G. Yang, Y. Yang, *Adv. Funct. Mater.* **2007**, *17*, 1636.
[39] M. Shakutsui, T. Iwamoto, R. Maeda, T. Tsutsui, K. Fujita, *Proc. SPIE-Int. Soc. Opt. Eng.* **2008**, *7052*, 705215.
[40] M. Shakutsui, T. Iwamoto, K. Fujita, *Jpn. J. Appl. Phys.* **2010**, *49*, 060207.
[41] S.-S. Kim, S.-I. Na, S.-J. Kang, D.-Y. Kim, *Sol. Energy Mater. Sol. Cells* **2010**, *94*, 171.
[42] J. Lee, T. Sagawa, S. Yoshikawa, *Thin Solid Films*, DOI: 10.1016/j.tsf.2012.07.080.
[43] B. Tremolet de Villers, C. J. Tassone, S. H. Tolbert, B. J. Schwartz, *J. Phys. Chem. C* **2009**, *113*, 18978.
[44] T. J. Prosa, M. J. Winokur, J. Moulton, P. Smith, A. J. Heeger, *Macromolecules* **1992**, *25*, 4364.

[45] C. W. T. Bulle-Lieuwma, W. J. H. van Genip, J. K. J. van Duren, P. Jonkheijm, R. A. J. Janssen, J. W. Niemantsverdriet, *Appl. Surf. Sci.* **2003**, *203*, 547.
[46] X. Yang, J. Loos, S. C. Veenstra, W. J. H. Verhees, M. M. Wienk, J. M. Kroon, M. A. J. Michels, R. A. J. Janssen, *Nano Lett.* **2005**, *5*, 579.
[47] T. Erb, U. Zhokhavets, G. Gobsch, S. Raleva, B. Stühn, P. Schilinsky, C. Waldauf, C. J. Brabec, *Adv. Funct. Mater.* **2005**, *15*, 1193–1196.
[48] S. S. van Bavel, M. Bärenklau, G. de With, H. Hoppe, J. Loos, *Adv. Funct. Mater.* **2010**, *20*, 1458.
[49] H. J. Snaith, A. C. Arias, A. C. Morteani, C. Silva, R. H. Friend, *Nano Lett.* **2002**, *2*, 1353.
[50] Y. Kim, S. Cook, S. A. Choulis, J. Nelson, J. R. Durrant, D. D. C. Bradley, *Chem. Mater.* **2004**, *16*, 4812.
[51] X. Yang, J. K. J. van Duren, R. A. J. Janssen, M. A. J. Michels, J. Loos, *Macromolecules* **2004**, *37*, 2151.
[52] A. Takahara, M. Morita, S. Sasaki, *SPring-8 Res. Front 2003* **2004**, 65.
[53] T. Sakurai, S. Toyosima, M. Kubota, T. Yamanari, T. Taima, K. Saito, K. Akimoto in *Photon Factory Activity Report*, **2007**, 4C/2007G182.
[54] C. R. McNeill, H. Frohne, J. L. Holdsworth, J. E. Furst, B. V. King, P. C. Dastoor, *Nano Lett.* **2004**, *4*, 219.

Received: August 31, 2012
Revised: October 18, 2012